Characterization and source apportionment of single particles from metalworking activities

Jovanna Arndt, Robert Healy, Ari Setyan, Pascal Flament, Karine Deboudt, Véronique Riffault, Laurent Alleman, Saliou Mbengue, John Wenger

Journal Pre-proof

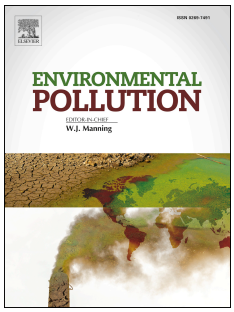

Characterization and source apportionment of single particles from metalworking activities

Jovanna Arndt, Robert M. Healy, Ari Setyan, Pascal Flament, Karine Deboudt, Véronique Riffault, Laurent Y. Alleman, Saliou Mbengue, John C. Wenger

PII: S0269-7491(20)36767-1

DOI: https://doi.org/10.1016/j.envpol.2020.116078

Reference: ENPO 116078

To appear in: *Environmental Pollution*

Received Date: 27 July 2020

Revised Date: 9 November 2020

Accepted Date: 10 November 2020

Please cite this article as: Arndt, J., Healy, R.M., Setyan, A., Flament, P., Deboudt, K., Riffault, V., Alleman, L.Y., Mbengue, S., Wenger, J.C., Characterization and source apportionment of single particles from metalworking activities, *Environmental Pollution*, https://doi.org/10.1016/j.envpol.2020.116078.

CRediT statement

Jovanna Arndt: Investigation, Methodology, Formal Analysis, Visualization, Data curation, Writing- original draft preparation. **Robert M. Healy**: Investigation, Methodology, Formal Analysis, Visualization, Writing- review and editing. **Ari Setyan**: Investigation, Methodology, Writing- review and editing. **Pascal Flament**: Conceptualization, Writing- review and editing, Supervision, Project Administration, Funding Acquisition. **Karine Deboudt**: Investigation, Conceptualization, Writing- review and editing. **Véronique Riffault**: Investigation, Formal Analysis, Conceptualization, Writing- review and editing, Supervision, Project Administration, Funding Acquisition. **Laurent Y. Alleman**: Investigation, Writing- review and editing. **Saliou Mbengue**: Investigation, Writing- review and editing. **John C. Wenger**: Conceptualization, Writing- review and editing, Supervision, Project Administration, Funding Acquisition

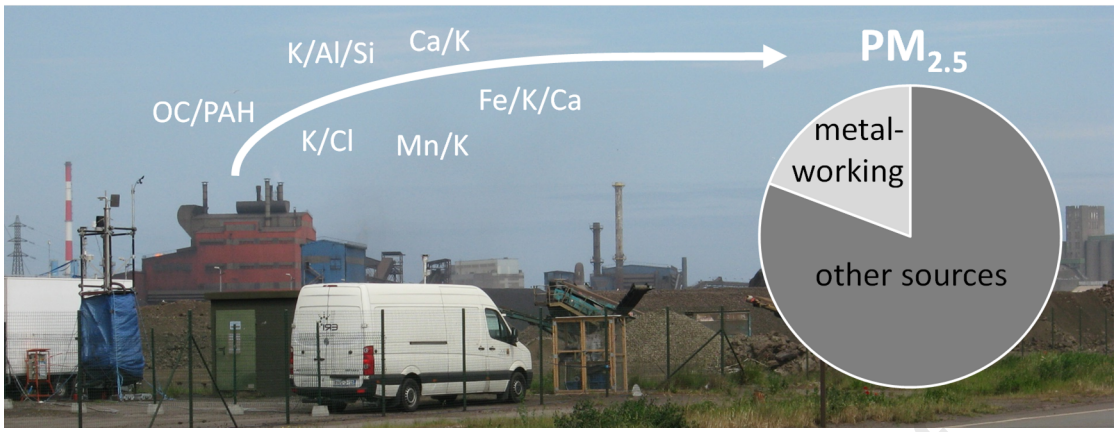

Characterization and source apportionment of single particles from metalworking activities

Jovanna Arndt[1], Robert M. Healy[2*], Ari Setyan[3,a,b], Pascal Flament[3], Karine Deboudt[3], Véronique Riffault[4], Laurent Y. Alleman[4], Saliou Mbengue[4,c], John C. Wenger[1]

[1]Department of Chemistry and Environmental Research Institute, University College Cork, Cork, Ireland

[2]Environmental Monitoring and Reporting Branch, Ontario Ministry of the Environment, Conservation and Parks, Toronto, Ontario, Canada

[3]Laboratoire de Physico-Chimie de l'Atmosphère, Université du Littoral Côte d'Opale, EA 4493-CNRS, 59140 Dunkerque, France

[4]IMT Lille Douai, Univ. Lille, SAGE - Sciences de l'Atmosphère et Génie de l'Environnement, F-59000 Lille, France

[a]now at: Empa, Swiss Federal Laboratories for Materials Science and Technology, Laboratory for Advanced Analytical Technologies, 8600 Dübendorf, Switzerland

[b]now at: ETH Zürich, Institute of Environmental Engineering, 8093 Zürich, Switzerland

[c]now at: CzechGlobe - Global Change Research Institute, Czech Academy of Sciences, 60300, Brno, Czech Republic

[*]Corresponding author contact details:

robert.healy@ontario.ca

Tel: +1 416 235 5764

Abstract

Industrial metalworking facilities emit a variety of air toxics including volatile organic compounds, polycyclic aromatic hydrocarbons (PAHs) and heavy metals. In order to investigate these emissions, a 1-month multi-instrument field campaign was undertaken at an industrial site in Grande-Synthe, Dunkirk (France), in May and June 2012. One of the main objectives of the study was to provide new information on the chemical composition of particulate matter with aerodynamic diameters smaller than 2.5 µm ($PM_{2.5}$) in the vicinity of metalworking facilities. An aerosol time-of-flight mass spectrometer (ATOFMS) was deployed to provide size-resolved chemical mixing state measurements of ambient single particles at high temporal resolution. This mixing state information was then used to apportion $PM_{2.5}$ to local metalworking facilities influencing the receptor site. Periods when the site was influenced by metalworking sources were characterised by a pronounced increase in particles containing toxic metals (manganese, iron, lead) and polycyclic aromatic hydrocarbons (PAHs) with a variety of chemical mixing states. The association of specific particle classes with a nearby ferromanganese alloy manufacturing plant was confirmed through comparison with previous analysis of raw materials (ores) and chimney filter particle samples collected at the facility. Particles associated with emissions from a nearby steelworks were also identified. The contribution of local metalworking activities to $PM_{2.5}$ at the receptor site for the period when the ATOFMS was deployed ranged from 1-65% with an average contribution of 17%, while the remaining mass was attributed to other local and regional sources. These findings demonstrate the impact of metalworking facilities on air quality downwind and provide useful single particle signatures for future source apportionment studies in communities impacted by metalworking emissions.

Keywords:

Particulate matter; source apportionment; mass spectrometry; industrial emissions; metalworking; air quality

1 Introduction

Negative health outcomes, lower crop yields, building damage and other impacts associated with industrial air pollution and greenhouse gas emissions were estimated to cost Europe over €300 billion between 2008 and 2012 (European Environment Agency, 2014). Almost a third of emissions of particulate matter with aerodynamic diameters smaller than 10 µm (PM_{10}) in France (CITEPA, 2014) are attributed to industrial sources. The city of Dunkirk lies in the Hauts de France region of Northern France and is home to over 200 industrial facilities from many sectors including refining and cement production. Dunkirk also contains one of Europe's largest steelworks, which emits approximately 3,000 t of PM per year (Flament et al., 2008). Numerous local industrial facilities generate plumes that impact air quality in the surrounding areas depending on local meteorological conditions, and local PM_{10} concentrations regularly exceed the European threshold value (24-hour average of 50 µg m^{-3}) (Setyan et al., 2019).

The physico-chemical nature of industrial PM varies considerably, particularly in terms of composition, depending on the type of industrial processes involved (Sanderson et al., 2014; Taiwo et al., 2014; Riffault et al., 2015). Ambient concentrations of particulate phase metals tend to be greater at locations directly influenced by industrial activities than at rural or urban locations (Osornio-Vargas Alvaro et al., 2003; Schaumann et al., 2004; Lim et al., 2010; Mohiuddin et al., 2014). Heavy metals and polycyclic aromatic hydrocarbons (PAHs) are important contributors to particle toxicity (Harrison and Yin, 2000). The generation of reactive oxygen species (ROS) and the development of asthma and cardiopulmonary disease have been linked to exposure to metals (Schaumann et al., 2004; Majestic et al., 2007). $PM_{2.5}$ collected from the same industrial area of Dunkirk investigated in this work has been recently demonstrated to damage DNA through an *in vitro* assessment of immortalized lung cells (Platel et al., 2020). Thus, the impact of industrial emissions on downwind air quality needs to be assessed in order to better understand human exposure to the associated air toxics.

Particulate PAH and metal content studies have been performed in the Dunkirk area previosuly due to the importance of metalworking sources and their proximity to large residential areas (Ledoux et al., 2006; Ledoux et al., 2009; Flament et al., 2008; Alleman et al., 2010; Marris et al., 2012; Marris et al., 2013; Hleis et al., 2013; Mbengue et al., 2014; Cazier et al., 2016; Crenn et al., 2018). In terms of source apportionment, the tracers used have included elemental ratios,

for examples Mn/Fe as a signature for a ferromanganese alloy metalworking facility, V/Ni for petrochemical facilities and isotopes of Pb and Fe as a signature for a local steelworks (Veron et al., 1999; Ledoux et al., 2006; Flament et al., 2008; Ledoux et al., 2009; Alleman et al., 2010; Marris et al., 2012). Emissions from the steelworks are also the dominant source of air emissions of Fe in Dunkirk, and the facility is estimated to emit 620 t of Fe annually (Flament et al., 2008). Anthropogenic particulate Fe emissions are of additional concern because of their higher solubility relative to Fe present in naturally occurring dust. Thus anthropogenic particulate Fe is more bioavailable than natural Fe dust, and the former can modulate primary productivity in high-nutrient, low chlorophyll (HNLC) ocean regions (Ito and Shi, 2016). Anthropogenic sources are responsible for approximately 7% of the 8.4 Mt of Fe deposited to oceans annually, and therefore have significant impacts upon carbon dioxide fixation globally (Wang et al., 2015).

The density and diversity of sources and emission profiles in Dunkirk complicates source apportionment efforts based on off-line analysis significantly (Alleman et al., 2010). One technique that is well suited to providing information on the size-resolved chemical composition and mixing state of particles emitted by industrial activities is single particle mass spectrometry. A review of industrial studies utilising this technique can be found in Riffault et al. (2015). The capability to provide mixing state information for individual particles is key to the role single particle mass spectrometry plays in source apportionment. Ambient particles containing specific internal mixtures of metals and other primary organic and inorganic species have been successfully assigned to their respective sources using this technique. For example, internally mixed Pb/Zn/Cl particles have been assigned to industrial waste incineration (Moffet et al., 2008b), Ga- and Se-containing particles particles have been associated with coal-fired power generation (Pekney et al., 2006; Snyder et al., 2009) and internally mixed V/Ni/sulfate particles have been associated with ship exhaust (Ault et al., 2009; Healy et al., 2009). Fe, Zn and Pb-containing particles have also been previously assigned to steelwork facility operations (Dall'Osto et al., 2008).

In this context, the NANO-INDUS field campaign was performed in the multi-industry influenced zone of Grande-Synthe in Dunkirk, France, close to a ferromanganese alloy facility and a steelworks (Setyan et al., 2019). An aerosol time-of-flight mass spectrometer (ATOFMS) was deployed to provide size-resolved chemical composition and mixing state data for industrial $PM_{2.5}$ with high temporal resolution. The ATOFMS data were used in combination with support

instrumentation measurements to apportion $PM_{2.5}$ to local and regional sources and to assess the impact of local metalworking facilities on air quality at the receptor site. Comparison of the ambient ATOFMS data with previous analysis of raw materials (ores) and particles collected on industrial filters from the ferromanganese alloy facility's chimneys (Arndt et al., 2016), enabled more effective source assignments for the particle classes observed during the field campaign.

2 Experimental

2.1 Sampling site and Instrumentation

All measurements were made in the industrial area of Grande-Synthe, Dunkirk (51.028809 N, 2.269448 E, 10 m above sea level), approximately 800 m southwest of a ferromanganese alloy manufacturing facility and 1 km southwest of a major steelworks (Figure S1). The adjacency of these two sources precludes separation of their air pollutant contributions based on wind direction alone (Setyan et al., 2019). Other nearby sources include a petrochemical storage facility <500 m to the west of the site and urban centres located to the east of the site (Fort-Mardyck and Dunkirk town centre, ~2 km and ~ 7 km from the site, respectively). The field campaign was undertaken from 15 May 2012 to 12 June 2012. An overview of the campaign, local meteorology, the instrumentation deployed and broad PM composition is described in detail elsewhere (Setyan et al., 2019). Date and time are reported in Coordinated Universal Time (UTC). $PM_{2.5}$ mass concentrations were determined every 2 hours with a MP101M Beta Gauge monitor. 24 to 48-hour filter samples were also collected on 25mm polycarbonate membrane filters (Whatman^{TM}) using 13- and 3-stage cascade impactors, and weighed with a micro-balance (UMT2, Mettler Toledo, Switzerland) (Mbengue et al., 2014, 2017).

The ATOFMS (TSI model 3800) was operated continuously from 18th May – 8th June 2012. A detailed description of the ATOFMS can be found elsewhere (Gard et al., 1997). Briefly, it consists of (i) an aerodynamic focusing lens (TSI AFL100) (Su et al., 2004) used to optimize particle transmission in the aerodynamic diameter (d_a) range 100-3000 nm, (ii) a particle sizing region, and (iii) a bipolar reflectron time-of-flight mass spectrometer. Single particles are desorbed/ionised using a pulsed Nd:YAG laser (λ = 266 nm, ~1 mJ pulse^{-1}) and positive and negative ion mass spectra of individual aerosol particles are simultaneously collected for successfully ionised particles. ATOFMS particle counts are scaled to account for sizing and other instrument biases as discussed below.

155

156 **2.2 ATOFMS Data Analysis**

157 Mass spectral data for over 800,000 single particles was collected using the ATOFMS during the
158 deployment period and was clustered using the *K*-means algorithm (*K*=80), as described
159 elsewhere (Gross et al., 2010; Healy et al., 2010; Healy et al., 2013). Clusters with similar mass
160 sepctral profiles, size distributions and temporality were combined. The final merged clusters
161 were then identified as particle "classes"; 33 in total. Approximately 15% of the particles ionised
162 did not produce positive ion mass spectra. The absence of positive ions is likely a result of
163 desorption/ionization matrix effects and precludes the assigment of these particles to a specific
164 category due to the absence of useful marker ions.

165 The particle class nomenclature used here is regularly used in the literature (Dall'Osto and
166 Harrison, 2006; Spencer et al., 2006; Ault et al., 2010; Pratt and Prather, 2012) and typically
167 denotes the dominant species in the positive ion mass spectra. For example, a particle class with
168 high intensities for sodium and elemental carbon is labelled Na-EC. In some cases this is
169 followed by secondary species detected in the negative ion mass spectra (e.g. EC-NH_4-NO_3),
170 referring to elemental carbon internally mixed with ammonium and nitrate.

171 The ATOFMS does not measure particle number or mass concentrations quantitatively, but
172 instead provides particle counts classified by aerodynamic diameter. The size-dependent
173 transmission efficiency of the focusing lens, data acquisition "busy time", and limited detection
174 of particles <150 nm complicate accurate counting of particles over the ATOFMS size range
175 (100-3000 nm d_a). The desorption/ionization laser used by the ATOFMS also complicates
176 quantitative speciation efforts. Differences in laser output power and variations in power density
177 across the laser beam between pulses (Steele et al., 2005; Wenzel and Prather, 2004) alter the
178 mass of each particle that is effectively desorbed impacting mass spectral signal intensities
179 (Gross et al., 2000a; Reinard and Johnston, 2008).

180 Thus the measured ATOFMS counts were scaled using two quantitative particle counting
181 instruments operated concurrently; an optical particle counter (OPC, TSI model 3300) and a
182 scanning mobility particle sizer (SMPS, TSI DMA model 3080 and CPC model 3010). Scaling
183 the ATOFMS number concentration data requires conversion of d_a (aerodynamic diameter) into
184 the corresponding volume equivalent diameter (d_{ve}), using the following relationship:

$$d_a = \frac{\rho_p}{\rho_0}\frac{d_{ve}}{\chi} \quad (1)$$

where ρ_p is the particle density, assumed for the purposes of number-size distribution scaling to be 1.7 g cm^{-3} as per previous applications of the method (Morawska et al., 1999; Reinard et al., 2007), d_{ve} is the volume equivalent diameter (operationally equivalent to electrical mobility diameter d_m measured by the SMPS and optical diameter d_o measured by the OPC), ρ_0 is standard density (1 g cm^{-3}) and χ represents the dynamic shape factor (e.g. 1, representing spherical shape). This is a simplified version of particle property relationships that are covered in detail elsewhere (DeCarlo et al., 2004). Mass concentrations can then be calculated from the scaled number concentrations as follows (Reinard et al., 2007):

$$m = \frac{\pi}{6}\rho_p d_{ve}^3 \quad (2)$$

The accuracy of the conversion of number concentrations to mass concentrations is dependent on the representativeness of χ and ρ_p for each type of particle. In the absence of morphology data χ is assumed to be 1. The use of a single density value, ρ_p, for conversion of ATOFMS scaled particle number concentrations to mass concentrations has previously resulted in good agreement with other quantitative measurements (Qin et al., 2006; Healy et al., 2013; Zhou et al., 2016). However, this simplification is not entirely accurate because different particle types exhibit different densities depending upon their chemical composition (Spencer and Prather, 2006; Reinard et al., 2007). A range of more representative densities, estimated from the bulk densities of the chemical components observed in the mass spectra (Bein et al., 2006; Reinard et al., 2007), was therefore used to convert the scaled number-size distributions to mass concentrations for each particle class, as listed in Table S1. ATOFMS-derived mass concentrations for $PM_{2.5}$ were averaged to hourly and 24 to 48-hour time resolutions for comparison with $PM_{2.5}$ measured concurrently on-line using the beta gauge instrument and off-line through gravimetric filter analysis, respectively. Similar ATOFMS-based source apportionment techniques have been performed previously to separate local and regional contributions to ambient PM in Paris, France and the apportionment results were found to agree well with those modelled using a regional chemical transport model (Healy et al., 2013; Skyllakou et al., 2014).

3 Results and Discussion

3.1 ATOFMS Results Overview

ATOFMS-derived mass concentrations of $PM_{2.5}$ were in reasonable temporal agreement with concurrently measured on-line beta gauge $PM_{2.5}$ mass concentrations at 2-hour resolution (R^2 = 0.62) and in good temporal agreement with gravimetric $PM_{2.5}$ mass concentrations at 24 to 48-hour resolution (R^2 = 0.91) as shown in Figure 1. This temporal agreement is in line with previous studies involving similar scaling procedures for single particle mass spectrometers (R^2 = 0.64-0.91) (Qin et al., 2006; Jeong et al., 2011; Healy et al., 2013; Zhou et al., 2016) and indicates that changes in ATOFMS-derived mass concentrations are representative of variations in ambient $PM_{2.5}$ mass concentrations at the site during the field study.

The 33 distinct ATOFMS particle classes identified through clustering were grouped into ten general "categories" for simplicity based on the dominant elements in their respective mass spectra. Briefly, the categories identified are: K-rich, EC-rich (elemental carbon), Na-rich, Fe-rich, Ca-rich, V-rich, Mn-rich, OC-rich (organic carbon), Pb-rich/Li-rich and Others. The relative contributions of each category in terms of mass concentration is shown in Table S1. The dominant categories are K-rich (24%), EC-rich (23%) Na-rich (10%) and Fe-rich (10%), followed by OC-rich (4%), Ca-rich (4%), V-rich (4%), Mn-rich (3%) and Pb-rich/Li-rich (3%). The "Others" category contains particle classes with minimal mass contributions (Sulfur and Amines, <1%). Temporal trends for each category are shown in Figure 2. It is clear from these temporal trends that the Na-rich, K-rich and EC categories exhibit prolonged, persistent mass contributions, consistent with regional background sources. Briefly, the K-rich category is dominated by a single particle class ($K\text{-}NO_3$) often associated with regional biomass combustion (Silva et al., 1999), routinely observed in regional background air in ATOFMS datasets collected across Europe (Dall'Osto et al., 2009; Healy et al., 2015; Arndt et al., 2017). The ATOFMS is highly sensitive to potassium (Gross et al., 2000a), and while the potassium ion is a dominant feature of biomass burning particle mass spectra, it is typically present as a trace component, with EC, OC and secondary inorganics dominating the composition in terms of mass (Healy et al., 2013). Particles in the EC-rich category are associated with various combustion sources, including vehicle exhaust and biomass burning (Spencer et al., 2006; Moffet et al., 2008a), and are often observed to be internally mixed with OC and secondary inorganics (Cahill et al., 2012; Healy et al., 2012). The Na-rich category is predominantly comprised of supermicron sea salt internally mixed with nitrate, which is expected for a coastal urban site (Gard et al., 1998). These three major particle categories are routinely observed in ATOFMS field studies. However,

several of the less abundant particle classes were found to be associated with local metalworking activities.

As outlined by Setyan et al. (2019), two distinct meteorological sea-breeze periods when winds were predominantly from the northeast were identified during the NANO-INDUS field campaign when the sampling site was downwind of the nearby ferromanganese and steelworks facilities (May 25-28 and June 02-03). During these events, particle number concentrations increased considerably, with concurrent increases in non-refractory chloride, organic aerosol and metals including manganese and iron. As shown in Figure 2, concentrations of several metal-rich particle categories detected by the ATOFMS were enhanced during these periods (shaded in grey). Particle classes associated with the ferromanganese alloy facility were identified through comparison with previous scanning electron microscopy/electron dispersive X-ray spectrometry (SEM-EDX) and ATOFMS analysis of raw materials (ores) and cooling, firing and smelting chimney filter samples previously collected at the facility (Arndt et al., 2016). Particle classes were assigned to the steelworks based on previous off-line elemental analysis of particles collected downwind of this facility (Mbengue et al., 2017) and previous ATOFMS measurements made in the vicinity of a large steelworks in the UK (Dall'Osto et al., 2008; Dall'Osto et al., 2012).

3.2 Metalworking Particle Source Identification

Temporal trends for individual particle classes exhibiting elevated concentrations during the prolonged periods when the site was downwind of the ferromanganese facility and the steelworks (Setyan et al., 2019) are shown in Figure 2. These include metal-rich particles with a variety of chemical mixing states and particles containing OC and polycyclic aromatic hydrocarbons (PAHs).

Mn-rich particles:

Three distinct Mn-containing particle classes were identified. Mn-K particles were characterized by the presence of Mn^+ (*m/z* 55) and K^+ (*m/z* 39) while Mn-Al-K particles exhibited a strong additional signal for aluminium (Al^+, *m/z* 27) and Mn-K-Fe particles exhibited a strong additional signal for iron (Fe^+, *m/z* 56) Average mass spectra for the three Mn-containing classes are shown in Figure 3, and the positive ion mass spectra are consistent with ATOFMS positive

ion mass spectra for particles collected at the ferromanganese facility (Arndt et al., 2016) (Figure S2). Mn-K particles are consistent with samples of the ores used at the facility as well as filter samples from the cooling chimney. Mn-Al-K particles also resemble both ore samples and the filter samples from the chimneys. Finally, Mn-K-Fe particle mass spectra are consistent with mass spectra for ore samples exclusively. Ambient Mn-K, Mn-Al-K and Mn-K-Fe are all enriched in nitrate (NO_2^-/NO_3^-, *m/z* -46/-62) and chloride (Cl^-, *m/z* -35) relative to the facility samples (Arndt et al., 2016), likely due to secondary accumulation of inorganic ions either through mixing with either inorganic gases from the metalworking facilities themselves or with ambient air after emission. All three Mn-rich particle classes are therefore assigned to the ferromanganese facility, which has been previously identified as the major local source of Mn in a previous apportionment study based on off-line filter analysis (Alleman et al., 2010).

Fe-rich particles:

Mass spectra for particles containing internally mixed iron, potassium and calcium (Fe-K-Ca) feature a dominant signal for Fe^+ (*m/z* 56) followed by K^+ (*m/z* 39), Ca^+ (*m/z* 40), Na^+ (*m/z* 23) and Al^+ (*m/z* 27) (Figure 4). Negative ion mass spectra contain peaks corresponding to chloride (Cl^-, *m/z* -35) and nitrate (NO_2^-/NO_3^-, *m/z* -46/-62). Fe-K-Na particles are quite similar to Fe-K-Ca particles, differing only in the intensities of sodium and potassium relative to iron. The mass spectral features of both particle classes are similar to internally mixed Fe/K/Ca particles collected from the chimneys of the ferromanganese facility (Arndt et al., 2016) (Figure S3), although the ambient particles shown in Figure 4 exhibit higher signals for nitrate (NO_2^-/NO_3^-, *m/z* -46/-62), again indicating uptake of nitrate after emission. While similarities exist between ambient and ferromanganese facility sample mass spectra for Fe-containing particles, the nearby steelworks remains the largest source of particulate iron in Dunkirk. A previous analysis of the steelworks particulate emissions demonstrated that most particles emitted were comprised of either Fe_2O_3, $CaCO_3$, KCl or were graphite flakes (Flament et al., 2008). Iron-rich particles similar to the ATOFMS Fe-K-Ca and Fe-K-Na classes were also detected by ATOFMS near a steelworks in Port Talbot (UK) (Dall'Osto et al., 2008), where they accounted for 3% of the particles detected and were attributed to the hot and cold mills. In the absence of any unique ions to differentiate between iron-containing particles from the steelworks and those emitted by the ferromanganese facility, and given that Fe/K/Ca particles only contributed a small fraction of the particles identified in the ferromanganese facility samples (Arndt et al., 2016), it is likely that the

majority of iron-containing particles detected during the field study originated from the steelworks. Setyan et al (2019) found that Mn/Fe elemental ratios in filter samples collected during the periods when the receptor site was downwind of the metalworking facilities were between the ratios expected for emissions from the ferromanganese facility and the steelworks, suggesting that emissions from both facilities were impacting the site. Contributions of Fe from both facilities were also observed in the previous source apportionment study (Alleman et al., 2010).

K-rich particles:

As shown in Figure 5, K-Cl particles are characterized by peaks for K^+ (*m/z* 39), Na^+ (*m/z* 23), Cl^- (*m/z* -35), and nitrate (NO_2^-/NO_3^-, *m/z* -46/-62). The local steelworks emits potassium chloride during the sintering process (Setyan et al., 2019), and potassium chloride emissions are estimated to represent ~40% of total sintering emissions from the facility (Flament et al., 2008; Hleis et al., 2013). K-Cl particles were not observed in the chimney filter or ore samples from the ferromanganese facility (Arndt et al., 2016). K-Cl particles have however, been detected downwind of the Port Talbot steelworks (Dall'Osto et al., 2008) and are thus assigned to the steelworks here. K-Al-Si particles are characterized by signals for K^+ (*m/z* 39), Na^+ (*m/z* 23), Fe^+ (*m/z* 56), AlO^- (*m/z* -43), $AlO(OH)^-/SiO_2^-/CO_3^-$ (*m/z* -60), SiO_3^- (*m/z* -76), $AlSiO_3^-$ (*m/z* -103), nitrate (NO_2^-/NO_3^-, *m/z* -46/-62), phosphate (PO_3^-, *m/z* -79), and chloride (Cl^-, *m/z* -35/-37) (Figure 5). No aluminium signal was observed in K-Al-Si positive mass spectra, likely due to matrix-related ion suppression (Reinard and Johnston, 2008). K-Cl and K-Al-Si particles were not observed in the ferromanganese facility samples and are therefore assigned to the steelworks. However, K-Al particles were positively identified in the ferromanganese facility firing chimney samples (Figure S4). Ambient K-Al particles produced stronger signals for nitrate (NO_2^-/NO_3^-, *m/z* -46/-62) and sulfate (HSO_4^-, *m/z* -97) but both the ambient and the firing chimney K-Al particles exhibited similar signals for F^- (*m/z* -19). Therefore fluoride represents a useful discriminatory marker for identifying potassium-containing particles from the ferromanganese facility.

Ca-rich particles:

Ca particles are characterized by a strong signal for Ca^+ (*m/z* 40) and smaller signals for Na^+ (*m/z* 23) and CaO^+(*m/z* 56), while Ca-K particles contain stronger signals for Na^+ (*m/z* 23) and K^+ (*m/z* 39) as shown in Figure 6. Based on comparison with the ferromanganese facility samples, both Ca and Ca-K particles appear to originate from the firing chimney, although ambient Ca-K particles exhibit higher signals for Na than the chimney samples (Figure S3). Negative ion mass spectra for both ambient Ca and Ca-K particles also exhibited higher signals for nitrate (NO_2^- /NO_3^-, *m/z* -46/-62) and sulfate (HSO_4^-, *m/z* -97) than their respective chimney sample particles again likely due to secondary accumulation after emission. A signal for fluoride is present in the ambient Ca negative ion mass spectra (F^-, *m/z* -19), consistent with the firing chimney samples, however this ion is absent in the ambient Ca-K particle spectra, indicating that ambient Ca-K particles may be associated with the steelworks instead. Flament et al. (2008) noted that calcium salts, including calcite and lime, are used in the sintering process at the steelworks, however the Ca-containing particles produced in that case are aggregates of Fe_2O_3, $CaCO_3$ and KCl. Ca-containing particles constituted only 8% of the particles analyzed from the steelworks sintering process by Flament et al. (2008), while Ca-rich particles accounted for approximately 80% of the particles in the firing chimney filter sample (Arndt et al., 2016). Ca-containing particles have also been assigned to the blast furnace unit of the Port Talbot steelworks (Taiwo et al., 2014), but those particles were also internally mixed with OC, and no Ca particles were reported in the previous Port Talbot steelworks studies by Dall'Osto et al. (2008,2012). Thus, while there remains a possibility that some of the Ca-rich particles could have originated from the steelworks, the ferromanganese facility is likely the dominant source.

OC-rich particles:

Three OC-containing particle classes were identified, of which the OC class was the dominant contributor in terms of mass. Average mass spectra are shown in Figure 7. All three classes are characterized by the presence of hydrocarbon fragments in the positive mass spectra (C_2H^{3+}/C_3H^+/$C_2H_3O^+$/$C_4H_3^+$/C_5H_3+/$C_6H_2^+$/$C_7H_3^+$, *m/z* 27/37/43/51/63/74/87) together with K^+ (*m/z* 39) and Na^+ (*m/z* 23). Carbon fragment ions (C^-/C_2^-/C_3^-…C_n^-, *m/z* -12/-24/-36....-12_n), CN^- (*m/z* -26) and sulfate (HSO_4^-, *m/z* -97) are evident in the negative mass spectra, while nitrate (NO_2^-/NO_3^-, *m/z* -46/-62) is dominant in the OC and PAH classes. The presence of internally mixed sulfate is consistent with emissions from the coke plant at the steelworks (Zhang et al., 2021). Mass spectra similar to the three OC-containing classes reported here were also observed

364 downwind of the Port Talbot steelworks (Dall'Osto et al., 2012), with *m/z* 202 assigned to
365 pyrene/fluoranthene as per previous ATOFMS field studies (Gross et al., 2000b). In the case of
366 Dall'Osto et al. (2012) OC-PAH particles were attributed to the hot and cold mills, while OC and
367 PAH particles were related to the steel/coke-making sector. Thus, all three organic carbon-
368 containing classes are attributed to the steelworks here.

369 **Pb-rich and Li-rich particles:**

370 Average ATOFMS mass spectra for Pb-rich particles are shown in Figure 8, characterized by
371 internally mixed K^+ (*m/z* 39), Pb^+ (*m/z* 208), Cl^- (*m/z* -35) and nitrate (NO_2^-/NO_3^-, *m/z* -46/-62).
372 No equivalent particles were observed in the ferromanganese facility samples. Pb-containing
373 particles similar to the Pb-rich class were also observed in the Port Talbot study, and represented
374 <1% of the particles ionized. In that case Pb-containing particles were assigned to the hot and
375 cold mills (Dall'Osto et al., 2008). The Port Talbot Pb-containing particles were internally mixed
376 with KCl, which is also the case for Dunkirk as shown in Figure 8. Thus Pb-rich particles are
377 attributed to the steelworks here.

378 Li-Zn particles contain Li^+ (*m/z* 7), Na^+ (*m/z* 23), K^+ (*m/z* 39), Zn^+ (*m/z* 65/66/68), nitrate (NO_2^-
379 /NO_3^-, *m/z* -46/-62) and phosphate (PO_3^-, *m/z* -79), as shown in Figure 8, and were not observed
380 in the ferromanganese facility samples. Particles detected by ATOFMS containing Li have been
381 assigned to coal combustion sources in previous studies (Guazzotti et al., 2003; Furutani et al.,
382 2011). Zn-containing particles were also associated with the Port Talbot steelworks, but those
383 particles did not contain internally mixed Li (Dall'Osto et al., 2008). Li-Zn particles have a
384 minimal mass contribution overall and it cannot be easily determined whether they originate
385 from the ferromanganese facility or the steelworks.

386 **3.3 Source Apportionment**

387 Summing the mass concentrations of the different particle classes associated with the
388 ferromanganese facility and the steelworks enabled an estimation of the $PM_{2.5}$ associated with
389 metalworking activities at the receptor site at hourly resolution. Elevated metalworking $PM_{2.5}$
390 concentrations are strongly dependent on northeasterly wind directions, consistent with the
391 locations of the two metalworking facilities (including ore and coal stockpiles), as shown in

Figure 9. Elevated non-metalworking (background) $PM_{2.5}$ mass concentrations are observed under northerly, easterly and southerly wind directions, consistent with more diffuse regional background sources. The contribution of metalworking activities to $PM_{2.5}$ at the receptor site ranged from 1-65% over the entire measurement period, with an average contribution of 17%. The average contribution for those periods when wind was predominantly from the northeast (shaded grey periods in Figure 2) is higher, at 28%. The overall average contribution of 17% is somewhat lower than the 28% contribution these two facilities were estimated to contribute to PM_{10} at a site approximately 3 km to the southeast through PMF analysis of filters collected in 2003-2005 (Alleman et al., 2010). Although the local metalworking facilities are not the dominant contributor to $PM_{2.5}$ mass at the receptor site, their dominant contributions to toxic metal and PAH-containing particle concentrations is of concern from an exposure perspective (Schroeder et al., 1987; Durant et al., 1996; Majestic et al., 2007; Zhang et al., 2008; Hu et al., 2012). The metalworking facilities were also the dominant contributor to ultrafine particles at the site (Setyan et al., 2019), a size fraction receiving increased attention with respect to its potential toxicological impacts (Ohlwein et al., 2019; Saleh et al., 2019; Sotty et al., 2019).

4 Conclusions

The unique particle mixing states associated with local metalworking facilities identified at the Dunkirk receptor site will be useful for future researchers aiming to apportion particulate matter to metalworking sources in other locations globally. The facilities investigated here use industrial processes that are common in the pyrometallurgic industry (sintering, smelting/reduction in an electric/blast furnace, refining, rolling and crushing of finished product) and therefore can be considered representative of that sector. The number of distinct chemical mixing states identified highlights the complexity and diversity in primary particle composition associated with emissions from metalworking. Particles containing Mn and Ca were associated predominantly with the ferromanganese facility, while particles containing Fe, K, Pb and PAHs were associated predominantly with the steelworks. Internally mixed fluoride was also found to be a useful discriminating marker for identifying ferromanganese firing chimney emissions specifically. The two metalworking facilities combined are estimated to contribute 17% on average to $PM_{2.5}$ mass concentrations at the receptor site during the measurement period, but are the dominant contributors of particles containing transition metals and PAHs; species associated with negative

health outcomes. The single particle source apportionment approach used here is also expected to be useful in other regions where the relative contributions of industrial emissions, including metalworking emissions, to ambient $PM_{2.5}$ concentrations need to be assessed. Knowledge of these contributions is particularly valuable for designing effective local air quality strategies.

CRediT statement

Jovanna Arndt: Investigation, Methodology, Formal Analysis, Visualization, Data curation, Writing- original draft preparation. **Robert M. Healy**: Investigation, Methodology, Formal Analysis, Visualization, Writing- review and editing. **Ari Setyan**: Investigation, Methodology, Writing- review and editing. **Pascal Flament**: Conceptualization, Writing- review and editing, Supervision, Project Administration, Funding Acquisition. **Karine Deboudt**: Investigation, Conceptualization, Writing- review and editing. **Véronique Riffault**: Investigation, Formal Analysis, Conceptualization, Writing- review and editing, Supervision, Project Administration, Funding Acquisition. **Laurent Y. Alleman**: Investigation, Writing- review and editing. **Saliou Mbengue**: Investigation, Writing- review and editing. **John C. Wenger**: Conceptualization, Writing- review and editing, Supervision, Project Administration, Funding Acquisition

Acknowledgements

Funding for the field measurements was provided by the French Agency of Environment and Energy Management (ADEME Grant #1181C0089). LPCA and IMT Lille Douai acknowledge financial support from the CaPPA (Chemical and Physical Properties of the Atmosphere) project funded by the French National Research Agency (ANR) through the PIA (Programme d'Investissement d'Avenir) under contract ANR-11-LABX-0005-01, and two CPER projects funded by the French Ministry of Higher Education and Research, the CNRS, the Regional Council “Hauts-de-France” and the European Regional Development Fund (ERDF): Climibio, and IRENI (additionally financed by the Communauté Urbaine de Dunkerque). We thank Vale Manganese France (VMF) for their collaboration in this study and Marc Fourmentin for

449 providing ultrasonic anemometer data. J.A. acknowledges support from the Irish Research
450 Council.

451

452 **References**

453 Alleman, L.Y., Lamaison, L., Perdrix, E., Robache, A., Galloo, J.-C., 2010. PM10 metal
454 concentrations and source identification using positive matrix factorization and wind sectoring in
455 a French industrial zone. Atmospheric Research 96, 612-625.

456 Arndt, J., Deboudt, K., Anderson, A., Blondel, A., Eliet, S., Flament, P., Fourmentin, M., Healy,
457 R.M., Savary, V., Setyan, A., Wenger, J.C., 2016. Scanning electron microscopy-energy
458 dispersive X-ray spectrometry (SEM-EDX) and aerosol time-of-flight mass spectrometry
459 (ATOFMS) single particle analysis of metallurgy plant emissions. Environmental Pollution 210,
460 9-17.

461 Arndt, J., Sciare, J., Mallet, M., Roberts, G.C., Marchand, N., Sartelet, K., Sellegri, K., Dulac, F.,
462 Healy, R.M., Wenger, J.C., 2017. Sources and mixing state of summertime background aerosol
463 in the north-western Mediterranean basin. Atmos. Chem. Phys. 17, 6975-7001.

464 Ault, A.P., Gaston, C.J., Wang, Y., Dominguez, G., Thiemens, M.H., Prather, K.A., 2010.
465 Characterization of the Single Particle Mixing State of Individual Ship Plume Events Measured
466 at the Port of Los Angeles. Environmental Science & Technology 44, 1954-1961.

467 Ault, A.P., Moore, M.J., Furutani, H., Prather, K.A., 2009. Impact of Emissions from the Los
468 Angeles Port Region on San Diego Air Quality during Regional Transport Events.
469 Environmental Science and Technology 43, 3500-3506.

470 Bein, K.J., Zhao, Y., Pekney, N.J., Davidson, C.I., Johnston, M.V., Wexler, A.S., 2006.
471 Identification of sources of atmospheric PM at the Pittsburgh Supersite--Part II: Quantitative
472 comparisons of single particle, particle number, and particle mass measurements. Atmospheric
473 Environment 40, 424-444.

474 Cahill, J.F., Suski, K., Seinfeld, J.H., Zaveri, R.A., Prather, K.A., 2012. The mixing state of
475 carbonaceous aerosol particles in northern and southern California measured during CARES and
476 CalNex 2010. Atmos. Chem. Phys. 12, 10989-11002.

477 Cazier, F., Genevray, P., Dewaele, D., Nouali, H., Verdin, A., Ledoux, F., Hachimi, A., Courcot,
478 L., Billet, S., Bouhsina, S., Shirali, P., Garçon, G., Courcot, D., 2016. Characterisation and
479 seasonal variations of particles in the atmosphere of rural, urban and industrial areas: Organic
480 compounds. Journal of Environmental Sciences 44, 45-56.

481 CITEPA, 2014. Inventaire des émissions de polluants atmosphériques et de gaz à effet

482 de serre en France – Format SECTEN.

483 Crenn, V., Chakraborty, A., Fronval, I., Petitprez, D., Riffault, V., 2018. Fine particles sampled
484 at an urban background site and an industrialized coastal site in Northern France—Part 2:
485 Comparison of offline and online analyses for carbonaceous aerosols. Aerosol Science and
486 Technology 52, 287-299.

Dall'Osto, M., Booth, M.J., Smith, W., Fisher, R., Harrison, R.M., 2008. A Study of the Size Distributions and the Chemical Characterization of Airborne Particles in the Vicinity of a Large Integrated Steelworks. Aerosol Science and Technology 42, 981-991.

Dall'Osto, M., Drewnick, F., Fisher, R., Harrison, R.M., 2012. Real-Time Measurements of Nonmetallic Fine Particulate Matter Adjacent to a Major Integrated Steelworks. Aerosol Science and Technology 46, 639-653.

Dall'Osto, M., Harrison, R.M., 2006. Chemical characterisation of single airborne particles in Athens (Greece) by ATOFMS. Atmospheric Environment 40, 7614-7631.

Dall'Osto, M., Harrison, R.M., Coe, H., Williams, P.I., Allan, J.D., 2009. Real time chemical characterization of local and regional nitrate aerosols. Atmos. Chem. Phys. 9, 3709-3720.

DeCarlo, P.F., Slowik, J.G., Worsnop, D.R., Davidovits, P., Jimenez, J.L., 2004. Particle morphology and density characterization by combined mobility and aerodynamic diameter measurements. Part 1: Theory. Aerosol Science & Technology 38, 1185-1205.

Durant, J.L., Busby, W.F., Lafleur, A.L., Penman, B.W., Crespi, C.L., 1996. Human cell mutagenicity of oxygenated, nitrated and unsubstituted polycyclic aromatic hydrocarbons associated with urban aerosols. Mutation Research/Genetic Toxicology 371, 123-157.

European Environment Agency, 2014. Costs of air pollution from European industrial

facilities 2008–2012 — an updated assessment.

Flament, P., Mattielli, N., Aimoz, L., Choël, M., Deboudt, K., Jong, J.d., Rimetz-Planchon, J., Weis, D., 2008. Iron isotopic fractionation in industrial emissions and urban aerosols. Chemosphere 73, 1793-1798.

Furutani, H., Jung, J., Miura, K., Takami, A., Kato, S., Kajii, Y., Uematsu, M., 2011. Single-particle chemical characterization and source apportionment of iron-containing atmospheric aerosols in Asian outflow. Journal of Geophysical Research: Atmospheres 116.

Gard, E., Mayer, J.E., Morrical, B.D., Dienes, T., Fergenson, D.P., Prather, K.A., 1997. Real-time analysis of individual atmospheric aerosol particles: Design and performance of a portable ATOFMS. Analytical Chemistry 69, 4083-4091.

Gard, E.E., Kleeman, M.J., Gross, D.S., Hughes, L.S., Allen, J.O., Morrical, B.D., Fergenson, D.P., Dienes, T., Galli, M.E., Johnson, R.J., Cass, G.R., Prather, K.A., 1998. Direct observation of heterogeneous chemistry in the atmosphere. Science 279, 1184-1187.

Gross, D.S., Atlas, R., Rzeszotarski, J., Turetsky, E., Christensen, J., Benzaid, S., Olsen, J., Smith, T., Steinberg, L., Sulman, J., Ritz, A., Anderson, B., Nelson, C., Musicant, D.R., Chen, L., Snyder, D.C., Schauer, J.J., 2010. Environmental chemistry through intelligent atmospheric data analysis. Environmental Modelling & Software 25, 760-769.

Gross, D.S., Galli, M.E., Silva, P.J., Prather, K.A., 2000a. Relative Sensitivity Factors for Alkali Metal and Ammonium Cations in Single-Particle Aerosol Time-of-Flight Mass Spectra. Analytical Chemistry 72, 416-422.

Gross, D.S., Galli, M.E., Silva, P.J., Wood, S.H., Liu, D.-Y., Prather, K.A., 2000b. Single Particle Characterization of Automobile and Diesel Truck Emissions in the Caldecott Tunnel. Aerosol Science & Technology 32, 152-163.

Guazzotti, S.A., Suess, D.T., Coffee, K.R., Quinn, P.K., Bates, T.S., Wisthaler, A., Hansel, A., Ball, W.P., Dickerson, R.R., Neusüß, C., Crutzen, P.J., Prather, K.A., 2003. Characterization of carbonaceous aerosols outflow from India and Arabia: Biomass/biofuel burning and fossil fuel combustion. J. Geophys. Res. 108.

Harrison, R.M., Yin, J., 2000. Particulate matter in the atmosphere: which particle properties are important for its effects on health? Science of The Total Environment 249, 85-101.

Healy, R.M., Evans, G.J., Murphy, M., Sierau, B., Arndt, J., McGillicuddy, E., O'Connor, I.P., Sodeau, J.R., Wenger, J.C., 2015. Single-particle speciation of alkylamines in ambient aerosol at five European sites. Analytical and Bioanalytical Chemistry 407, 5899-5909.

Healy, R.M., Hellebust, S., Kourtchev, I., Allanic, A., O'Connor, I.P., Bell, J.M., Healy, D.A., Sodeau, J.R., Wenger, J.C., 2010. Source apportionment of PM2.5 in Cork Harbour, Ireland using a combination of single particle mass spectrometry and quantitative semi-continuous measurements. Atmos. Chem. Phys. 10, 9593-9613.

Healy, R.M., O'Connor, I.P., Hellebust, S., Allanic, A., Sodeau, J.R., Wenger, J.C., 2009. Characterisation of single particles from in-port ship emissions. Atmospheric Environment 43, 6408-6414.

Healy, R.M., Sciare, J., Poulain, L., Crippa, M., Wiedensohler, A., Prévôt, A.S.H., Baltensperger, U., Sarda-Estève, R., McGuire, M.L., Jeong, C.H., McGillicuddy, E., O'Connor, I.P., Sodeau, J.R., Evans, G.J., Wenger, J.C., 2013. Quantitative determination of carbonaceous particle mixing state in Paris using single-particle mass spectrometer and aerosol mass spectrometer measurements. Atmos. Chem. Phys. 13, 9479-9496.

Healy, R.M., Sciare, J., Poulain, L., Kamili, K., Merkel, M., Müller, T., Wiedensohler, A., Eckhardt, S., Stohl, A., Sarda-Estève, R., McGillicuddy, E., O'Connor, I.P., Sodeau, J.R., Wenger, J.C., 2012. Sources and mixing state of size-resolved elemental carbon particles in a European megacity: Paris. Atmosperic Chemistry & Physics 12, 1681-1700.

Hleis, D., Fernandez-Olmo, I., Ledoux, F., Kfoury, A., Courcot, L., Desmonts, T., Courcot, D., 2013. Chemical profile identification of fugitive and confined particle emissions from an integrated iron and steelmaking plant. Journal of Hazardous Materials 250-251, 246-255.

Hu, X., Zhang, Y., Ding, Z., Wang, T., Lian, H., Sun, Y., Wu, J., 2012. Bioaccessibility and health risk of arsenic and heavy metals (Cd, Co, Cr, Cu, Ni, Pb, Zn and Mn) in TSP and PM2.5 in Nanjing, China. Atmospheric Environment 57, 146-152.

Ito, A., Shi, Z., 2016. Delivery of anthropogenic bioavailable iron from mineral dust and combustion aerosols to the ocean. Atmos. Chem. Phys. 16, 85-99.

Jeong, C.H., McGuire, M.L., Godri, K.J., Slowik, J.G., Rehbein, P.J.G., Evans, G.J., 2011. Quantification of aerosol chemical composition using continuous single particle measurements. Atmos. Chem. Phys. 11, 7027-7044.

Ledoux, F., Courcot, D., Courcot, L., Aboukais, A., Puskaric, E., 2009. Atmospheric aerosols behaviour at an industrial area in Northern France. Int. J. Environ. Pollut. 39, 286-305.

Ledoux, F., Laversin, H., Courcot, D., Courcot, L., Zhilinskaya, E.A., Puskaric, E., Aboukaïs, A., 2006. Characterization of iron and manganese species in atmospheric aerosols from anthropogenic sources. Atmospheric Research 82, 622-632.

Lim, J.-M., Lee, J.-H., Moon, J.-H., Chung, Y.-S., Kim, K.-H., 2010. Airborne PM10 and metals from multifarious sources in an industrial complex area. Atmospheric Research 96, 53-64.

Majestic, B.J., Schauer, J.J., Shafer, M.M., 2007. Development of a Manganese Speciation Method for Atmospheric Aerosols in Biologically and Environmentally Relevant Fluids. Aerosol Science and Technology 41, 925-933.

Marris, H., Deboudt, K., Augustin, P., Flament, P., Blond, F., Fiani, E., Fourmentin, M., Delbarre, H., 2012. Fast changes in chemical composition and size distribution of fine particles during the near-field transport of industrial plumes. Science of The Total Environment 427-428, 126-138.

Marris, H., Deboudt, K., Flament, P., Grobéty, B., Gieré, R., 2013. Fe and Mn Oxidation States by TEM-EELS in Fine-Particle Emissions from a Fe-Mn Alloy Making Plant. Environmental Science & Technology 47, 10832-10840.

Mbengue, S., Alleman, L.Y., Flament, P., 2014. Size-distributed metallic elements in submicronic and ultrafine atmospheric particles from urban and industrial areas in northern France. Atmospheric Research 135–136, 35-47.

Mbengue, S., Alleman, L.Y., Flament, P., 2017. Metal-bearing fine particle sources in a coastal industrialized environment. Atmospheric Research 183, 202-211.

Moffet, R.C., de Foy, B., Molina, L.T., Molina, M.J., Prather, K.A., 2008a. Measurement of ambient aerosols in northern Mexico City by single particle mass spectrometry. Atmos. Chem. Phys. 8, 4499-4516.

Moffet, R.C., Desyaterik, Y., Hopkins, R.J., Tivanski, A.V., Gilles, M.K., Wang, Y., Shutthanandan, V., Molina, L.T., Abraham, R.G., Johnson, K.S., Mugica, V., Molina, M.J., Laskin, A., Prather, K.A., 2008b. Characterization of Aerosols Containing Zn, Pb, and Cl from an Industrial Region of Mexico City. Environmental Science and Technology 42, 7091-7097.

Mohiuddin, K., Strezov, V., Nelson, P.F., Stelcer, E., 2014. Characterisation of trace metals in atmospheric particles in the vicinity of iron and steelmaking industries in Australia. Atmospheric Environment 83, 72-79.

Morawska, L., Johnson, G., Ristovski, Z.D., Agranovski, V., 1999. Relation between particle mass and number for submicrometer airborne particles. Atmospheric Environment 33, 1983-1990.

Ohlwein, S., Kappeler, R., Kutlar Joss, M., Künzli, N., Hoffmann, B., 2019. Health effects of ultrafine particles: a systematic literature review update of epidemiological evidence. International Journal of Public Health 64, 547-559.

Osornio-Vargas Alvaro, R., Bonner James, C., Alfaro-Moreno, E., Martínez, L., García-Cuellar, C., Ponce-de-León Rosales, S., Miranda, J., Rosas, I., 2003. Proinflammatory and cytotoxic effects of Mexico City air pollution particulate matter in vitro are dependent on particle size and composition. Environmental Health Perspectives 111, 1289-1293.

Pekney, N.J., Davidson, C.I., Bein, K.J., Wexler, A.S., Johnston, M.V., 2006. Identification of sources of atmospheric PM at the Pittsburgh Supersite, Part I: Single particle analysis and filter-based positive matrix factorization. Atmospheric Environment 40, 411-423.

Petit, J.E., Favez, O., Albinet, A., Canonaco, F., 2017. A user-friendly tool for comprehensive evaluation of the geographical origins of atmospheric pollution: Wind and trajectory analyses. Environ. Modell. Softw. 88, 183-187.

Platel, A., Privat, K., Talahari, S., Delobel, A., Dourdin, G., Gateau, E., Simar, S., Saleh, Y., Sotty, J., Antherieu, S., Canivet, L., Alleman, L.Y., Perdrix, E., Garçon, G., Denayer, F.O., Lo Guidice, J.M., Nesslany, F., 2020. Study of in vitro and in vivo genotoxic effects of air pollution fine (PM2.5-0.18) and quasi-ultrafine (PM0.18) particles on lung models. Science of The Total Environment 711, 134666.

Pratt, K.A., Prather, K.A., 2012. Mass spectrometry of atmospheric aerosols—Recent developments and applications. Part II: On-line mass spectrometry techniques. Mass Spectrometry Reviews 31, 17-48.

Qin, X., Bhave, P.V., Prather, K.A., 2006. Comparison of Two Methods for Obtaining Quantitative Mass Concentrations from Aerosol Time-of-Flight Mass Spectrometry Measurements. Analytical Chemistry 78, 6169-6178.

Reinard, M.S., Adou, K., Martini, J.M., Johnston, M.V., 2007. Source characterization and identification by real-time single particle mass spectrometry. Atmospheric Environment 41, 9397-9409.

Reinard, M.S., Johnston, M.V., 2008. Ion Formation Mechanism in Laser Desorption Ionization of Individual Nanoparticles. Journal of the American Society for Mass Spectrometry 19, 389-399.

Riffault, V., Arndt, J., Marris, H., Mbengue, S., Setyan, A., Alleman, L.Y., Deboudt, K., Flament, P., Augustin, P., Delbarre, H., Wenger, J., 2015. Fine and Ultrafine Particles in the Vicinity of Industrial Activities: A Review. Critical Reviews in Environmental Science and Technology 45, 2305-2356.

Saleh, Y., Antherieu, S., Dusautoir, R., Y Alleman, L., Sotty, J., De Sousa, C., Platel, A., Perdrix, E., Riffault, V., Fronval, I., Nesslany, F., Canivet, L., Garçon, G., Lo-Guidice, J.-M., 2019. Exposure to Atmospheric Ultrafine Particles Induces Severe Lung Inflammatory Response and Tissue Remodeling in Mice. International journal of environmental research and public health 16, 1210.

Sanderson, P., Delgado-Saborit, J.M., Harrison, R.M., 2014. A review of chemical and physical characterisation of atmospheric metallic nanoparticles. Atmospheric Environment 94, 353-365.

Schaumann, F., Borm, P.J.A., Herbrich, A., Knoch, J., Pitz, M., Schins, R.P.F., Luettig, B., Hohlfeld, J.M., Heinrich, J., Krug, N., 2004. Metal-rich Ambient Particles (Particulate Matter2.5) Cause Airway Inflammation in Healthy Subjects. American Journal of Respiratory and Critical Care Medicine 170, 898-903.

Schroeder, W.H., Dobson, M., Kane, D.M., Johnson, N.D., 1987. Toxic Trace Elements Associated with Airborne Particulate Matter: A Review. JAPCA 37, 1267-1285.

Setyan, A., Flament, P., Locoge, N., Deboudt, K., Riffault, V., Alleman, L.Y., Schoemaecker, C., Arndt, J., Augustin, P., Healy, R.M., Wenger, J.C., Cazier, F., Delbarre, H., Dewaele, D., Dewalle, P., Fourmentin, M., Genevray, P., Gengembre, C., Leonardis, T., Marris, H., Mbengue, S., 2019. Investigation on the near-field evolution of industrial plumes from metalworking activities. Science of The Total Environment 668, 443-456.

650 Silva, P.J., Liu, D.Y., Noble, C.A., Prather, K.A., 1999. Size and chemical characterization of
651 individual particles resulting from biomass burning of local Southern California species.
652 Environmental Science & Technology 33, 3068-3076.

653 Skyllakou, K., Murphy, B.N., Megaritis, A.G., Fountoukis, C., Pandis, S.N., 2014. Contributions
654 of local and regional sources to fine PM in the megacity of Paris. Atmos. Chem. Phys. 14, 2343-
655 2352.

656 Snyder, D.C., Schauer, J.J., Gross, D.S., Turner, J.R., 2009. Estimating the contribution of point
657 sources to atmospheric metals using single-particle mass spectrometry. Atmospheric
658 Environment 43, 4033-4042.

659 Sotty, J., Garçon, G., Denayer, F.O., Alleman, L.Y., Saleh, Y., Perdrix, E., Riffault, V., Dubot,
660 P., Lo-Guidice, J.M., Canivet, L., 2019. Toxicological effects of ambient fine (PM2.5-0.18) and
661 ultrafine (PM0.18) particles in healthy and diseased 3D organo-typic mucocilary-phenotype
662 models. Environmental Research 176, 108538.

663 Spencer, M., Prather, K., 2006. Using ATOFMS to Determine OC/EC Mass Fractions in
664 Particles. Aerosol Science & Technology 40, 585-594.

665 Spencer, M.T., Shields, L.G., Sodeman, D.A., Toner, S.M., Prather, K.A., 2006. Comparison of
666 oil and fuel particle chemical signatures with particle emissions from heavy and light duty
667 vehicles. Atmospheric Environment 40, 5224-5235.

668 Steele, P.T., Srivastava, A., Pitesky, M.E., Fergenson, D.P., Tobias, H.J., Gard, E.E., Frank, M.,
669 2005. Desorption/Ionization Fluence Thresholds and Improved Mass Spectral Consistency
670 Measured Using a Flattop Laser Profile in the Bioaerosol Mass Spectrometry of Single Bacillus
671 Endospores. Analytical Chemistry 77, 7448-7454.

672 Su, Y., Sipin, M.F., Furutani, H., Prather, K.A., 2004. Development and Characterization of an
673 Aerosol Time-of-Flight Mass Spectrometer with Increased Detection Efficiency. Analytical
674 Chemistry 76, 712-719.

675 Taiwo, A.M., Harrison, R.M., Shi, Z., 2014. A review of receptor modelling of industrially
676 emitted particulate matter. Atmospheric Environment 97, 109-120.

677 Veron, A., Flament, P., Bertho, M.L., Alleman, L., Flegal, R., Hamelin, B., 1999. Isotopic
678 evidence of pollutant lead sources in Northwestern France. Atmospheric Environment 33, 3377-
679 3388.

680 Wang, R., Balkanski, Y., Boucher, O., Bopp, L., Chappell, A., Ciais, P., Hauglustaine, D.,
681 Peñuelas, J., Tao, S., 2015. Sources, transport and deposition of iron in the global atmosphere.
682 Atmos. Chem. Phys. 15, 6247-6270.

683 Wenzel, R.J., Prather, K.A., 2004. Improvements in ion signal reproducibility obtained using a
684 homogeneous laser beam for on-line laser desorption/ionization of single particles. Rapid
685 Communications in Mass Spectrometry 18, 1525-1533.

686 Zhang, S., Tison, E., Dusanter, S., Beaugard, C., Gengembre, C., Augustin, P., Fourmentin, M.,
687 Delbarre, H., Riffault, V., 2021. Near real-time PM1 chemical composition measurements at a
688 French urban background and coastal site under industrial influence over more than a year:
689 Temporal variability and assessment of sulfur-containing emissions. Atmospheric Environment
690 244, 117960.

Zhang, Y., Schauer, J.J., Shafer, M.M., Hannigan, M.P., Dutton, S.J., 2008. Source Apportionment of in Vitro Reactive Oxygen Species Bioassay Activity from Atmospheric Particulate Matter. Environmental Science & Technology 42, 7502-7509.

Zhou, Y., Huang, X.H.H., Griffith, S.M., Li, M., Li, L., Zhou, Z., Wu, C., Meng, J., Chan, C.K., Louie, P.K.K., Yu, J.Z., 2016. A field measurement based scaling approach for quantification of major ions, organic carbon, and elemental carbon using a single particle aerosol mass spectrometer. Atmospheric Environment 143, 300-312.

718 **Figures**

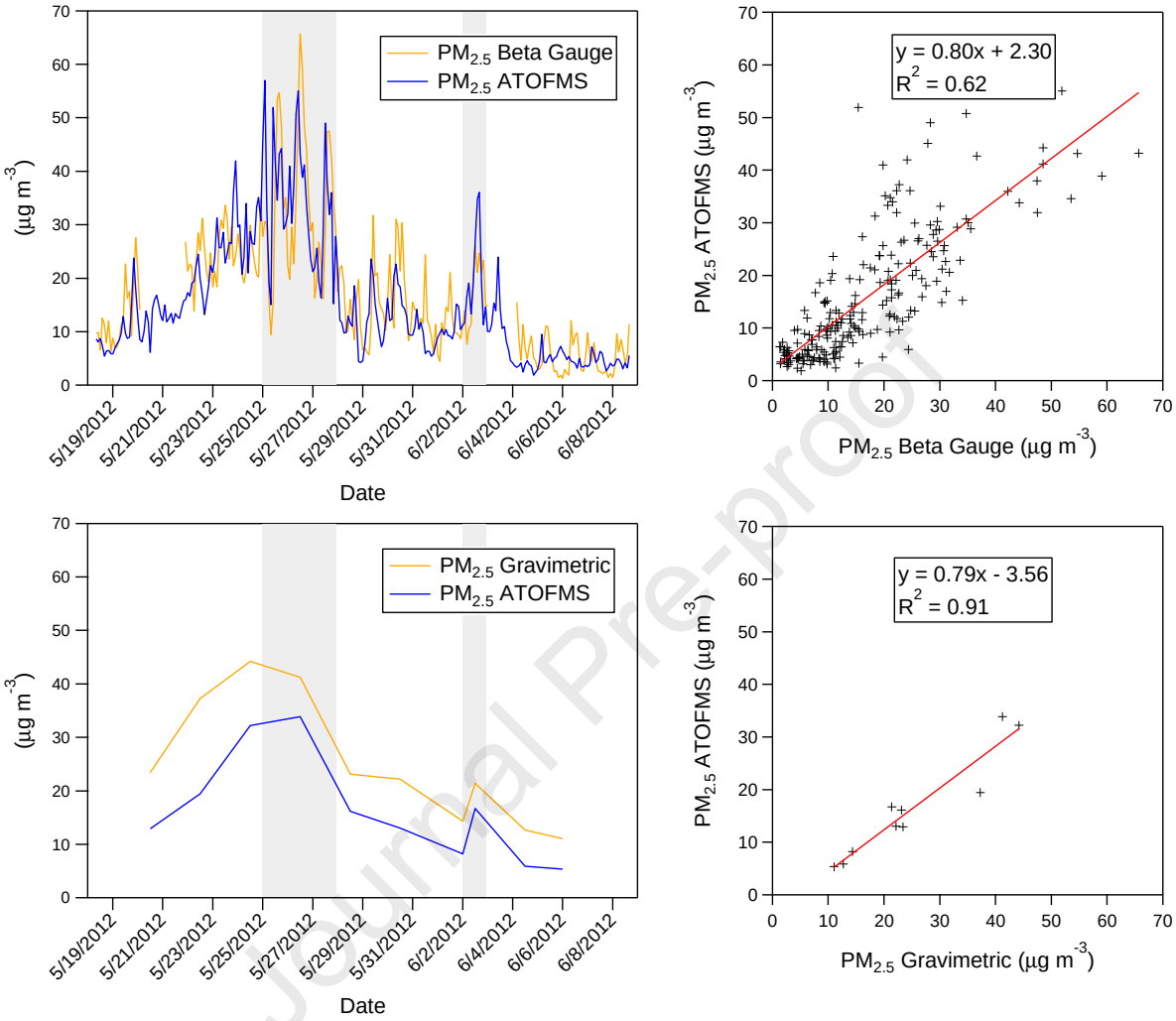

719

720 Figure 1: Top: Comparison of 2-hour mass concentrations of $PM_{2.5}$ measured by the beta gauge
721 instrument and derived using the ATOFMS. Bottom: Comparison of 24 to 48-hour mass
722 concentrations of $PM_{2.5}$ determined by gravimetric filter analysis and derived using the
723 ATOFMS. Red lines represent least squares regression fits. Days when wind was predominantly
724 from the northeast (the direction of metalworking facilities) are shaded grey.

725

726

727

728

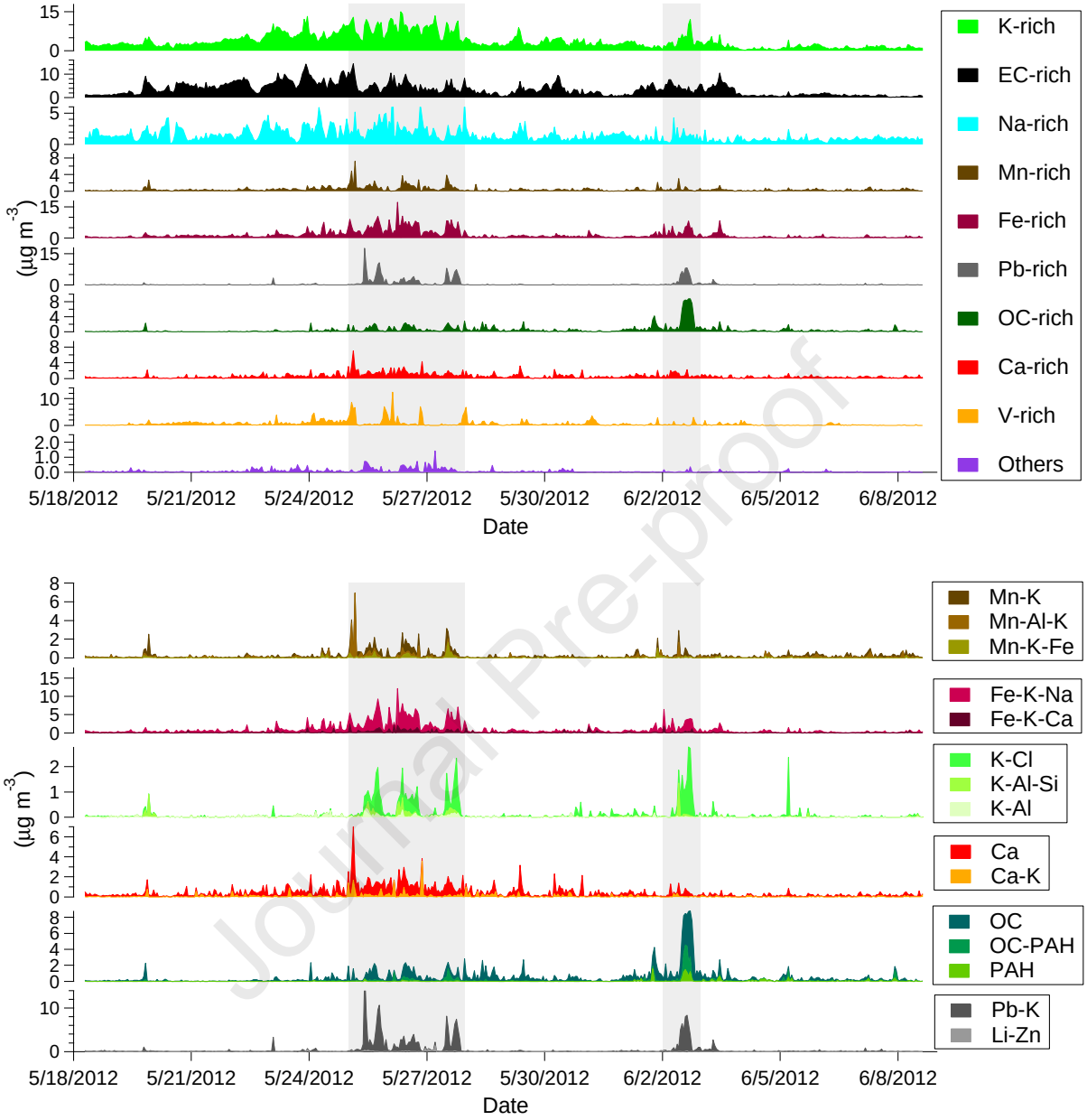

Figure 2: Top: Temporal trends of hourly resolution mass concentrations of the ten ATOFMS particle categories. Bottom: Temporal trends of hourly resolution mass concentrations of metalworking ATOFMS particle classes. Days when wind was predominantly from the northeast (the direction of metalworking facilities) are shaded grey.

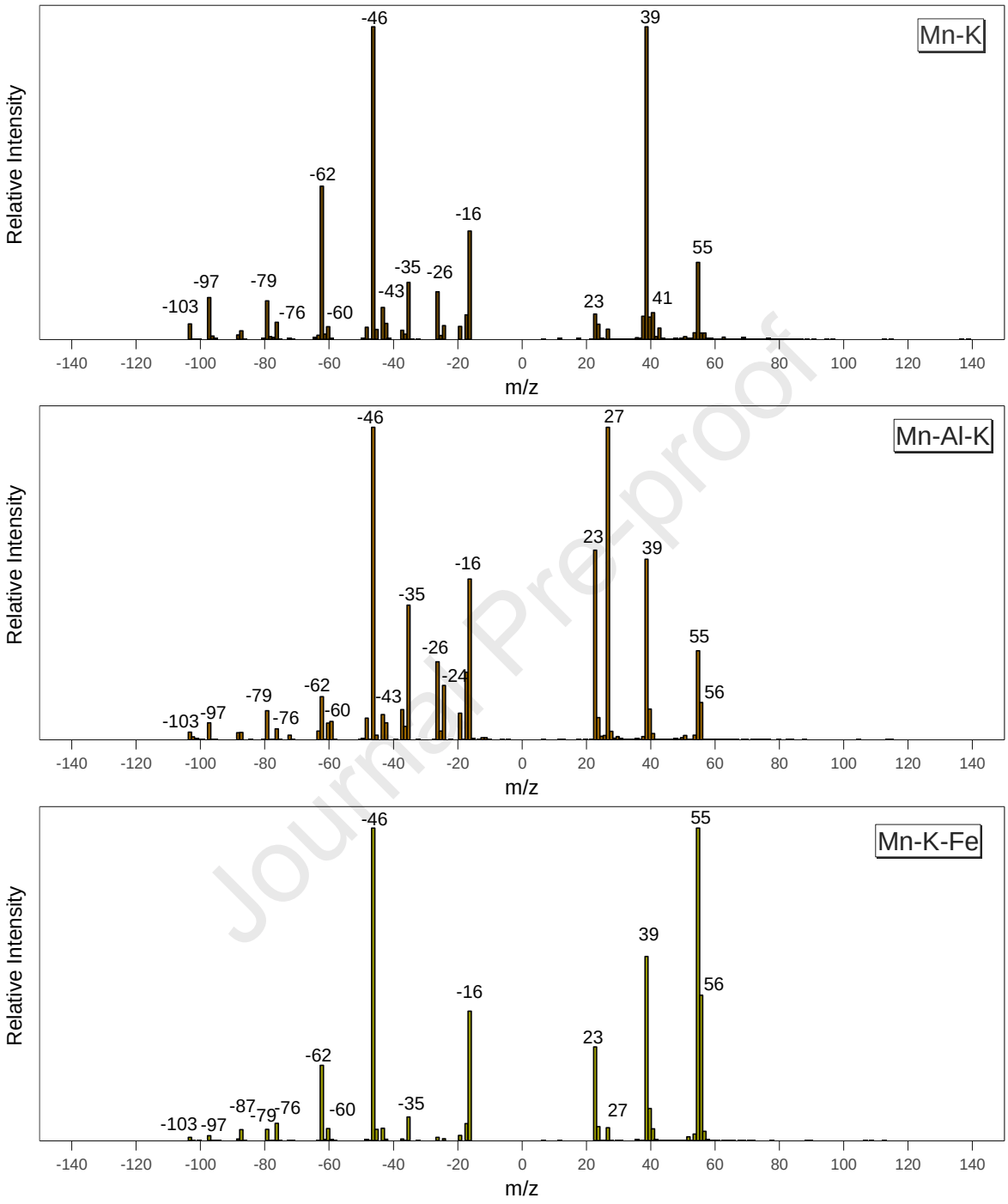

735

736 Figure 3: Average mass spectra for Mn-rich metalworking particle classes.

737

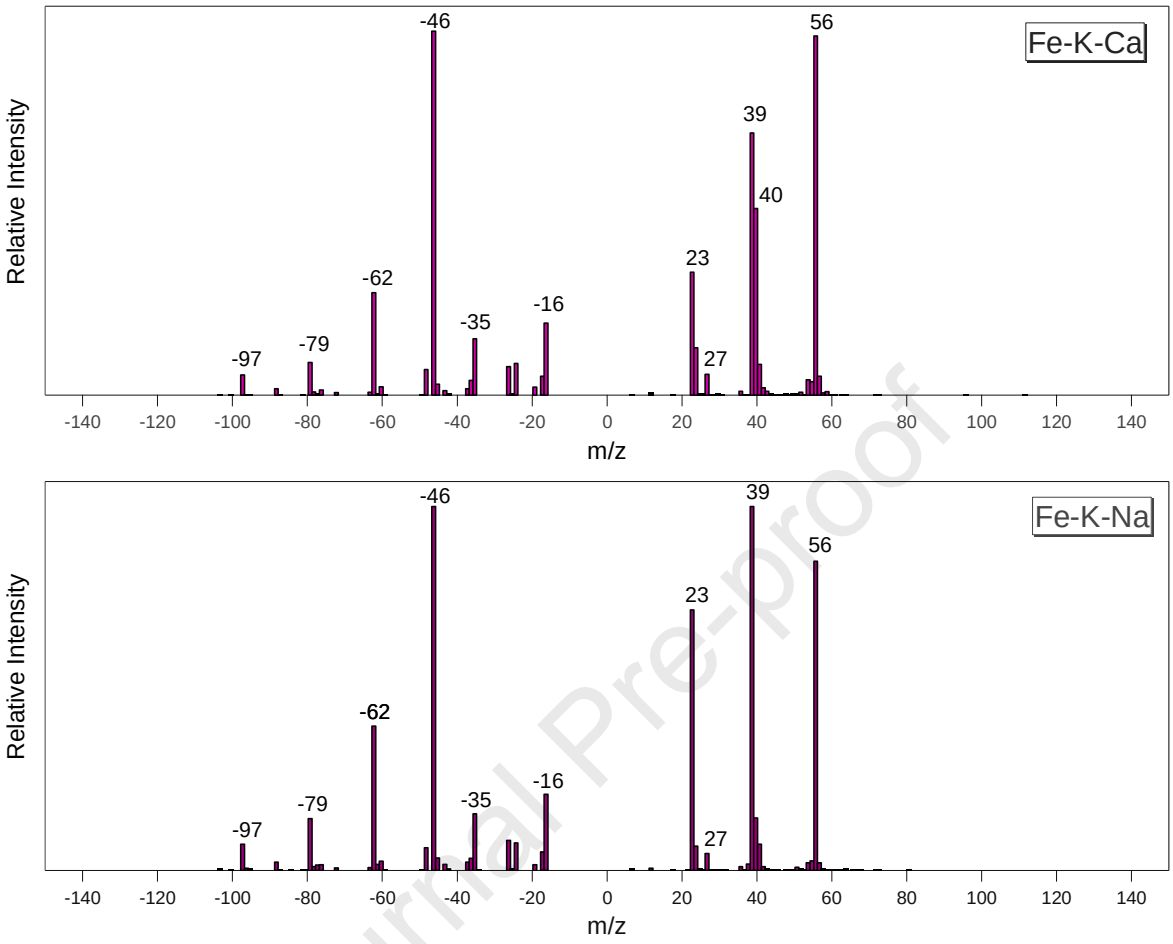

738

739 Figure 4: Average mass spectra for iron-rich metalworking particle classes.

740

741

742

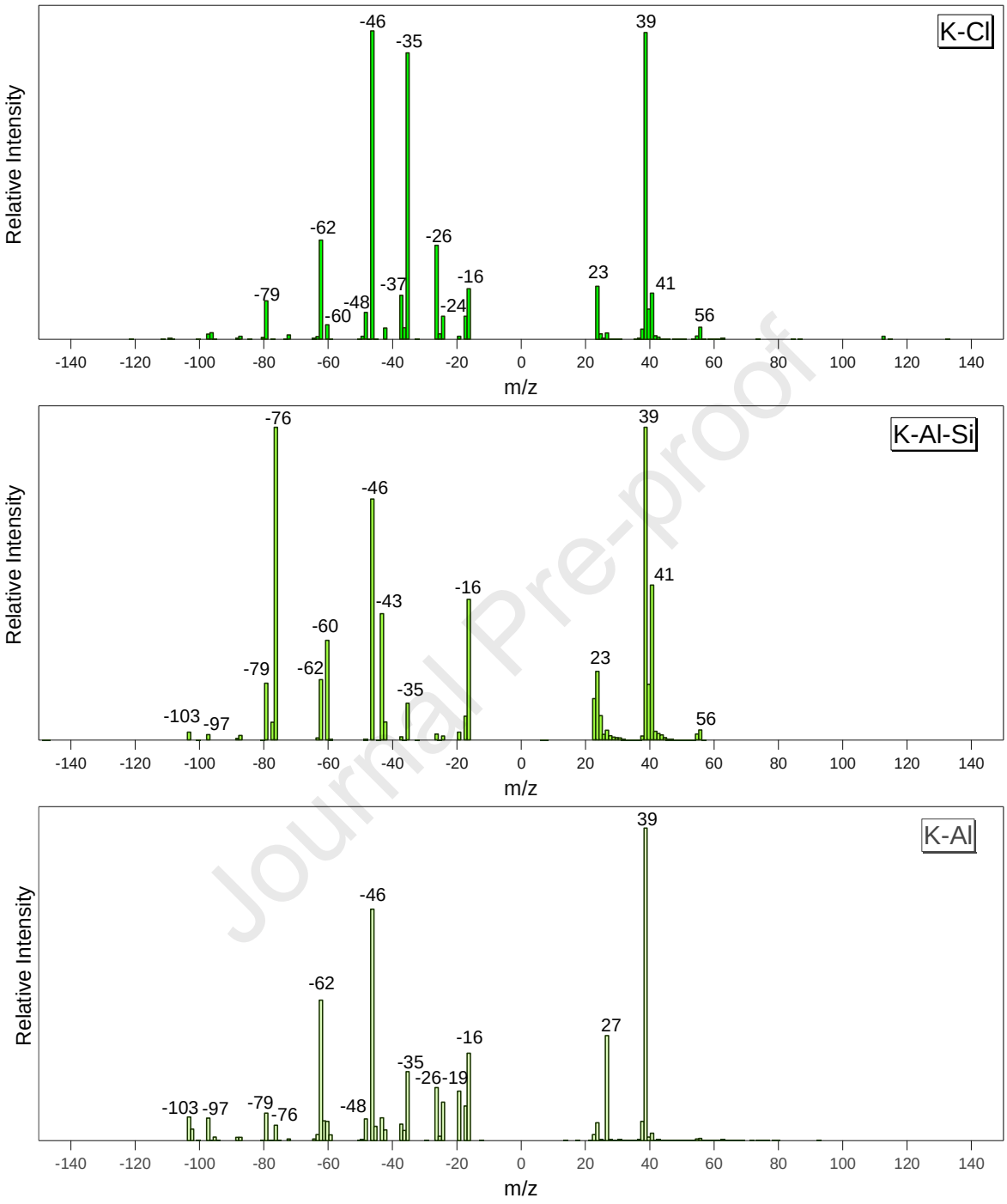

743

744 Figure 5: Average mass spectra for K-rich metalworking particle classes.

745

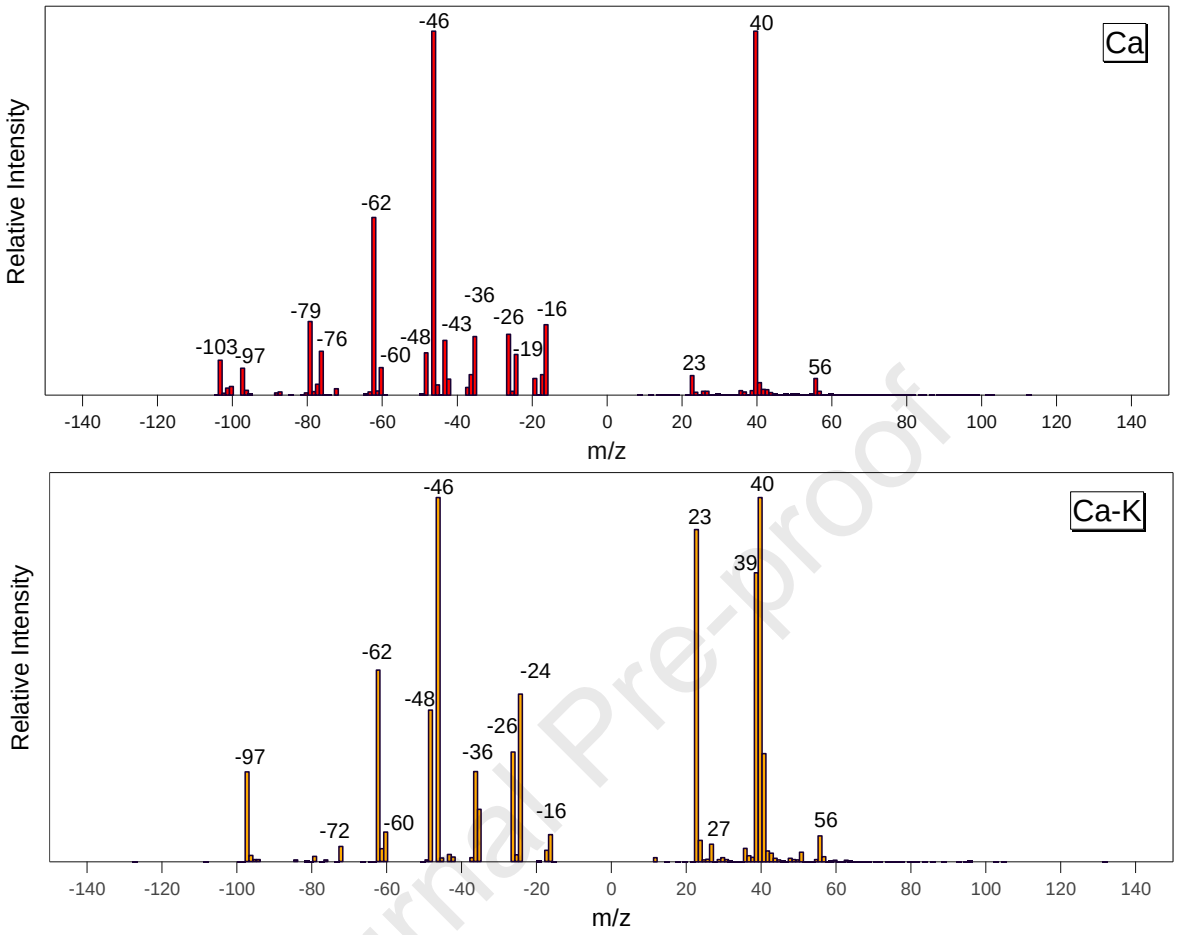

Figure 6: Average mass spectra for Ca-rich metalworking particle classes.

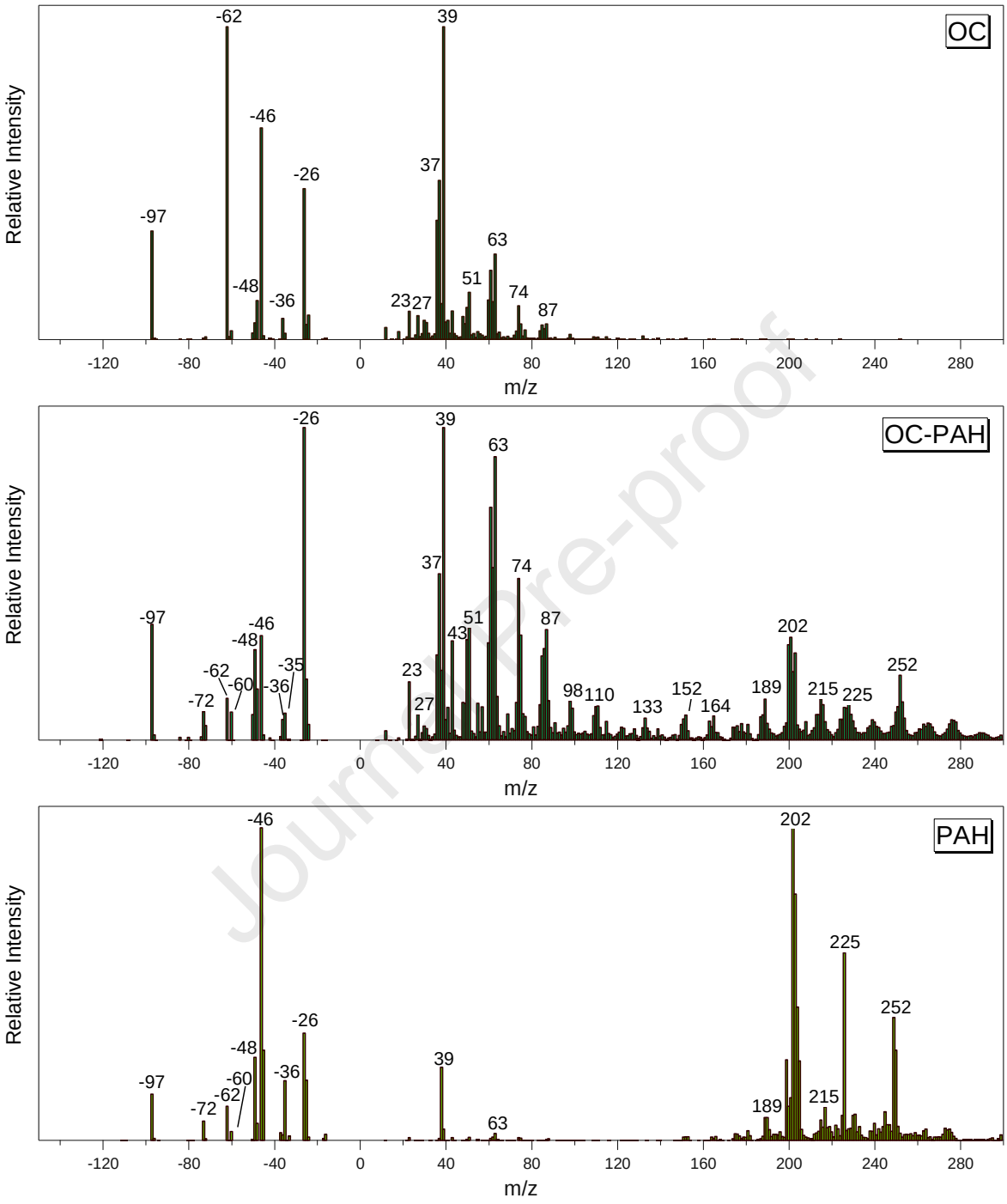

752

753 Figure 7: Average mass spectra for OC-rich metalworking particle classes.

754

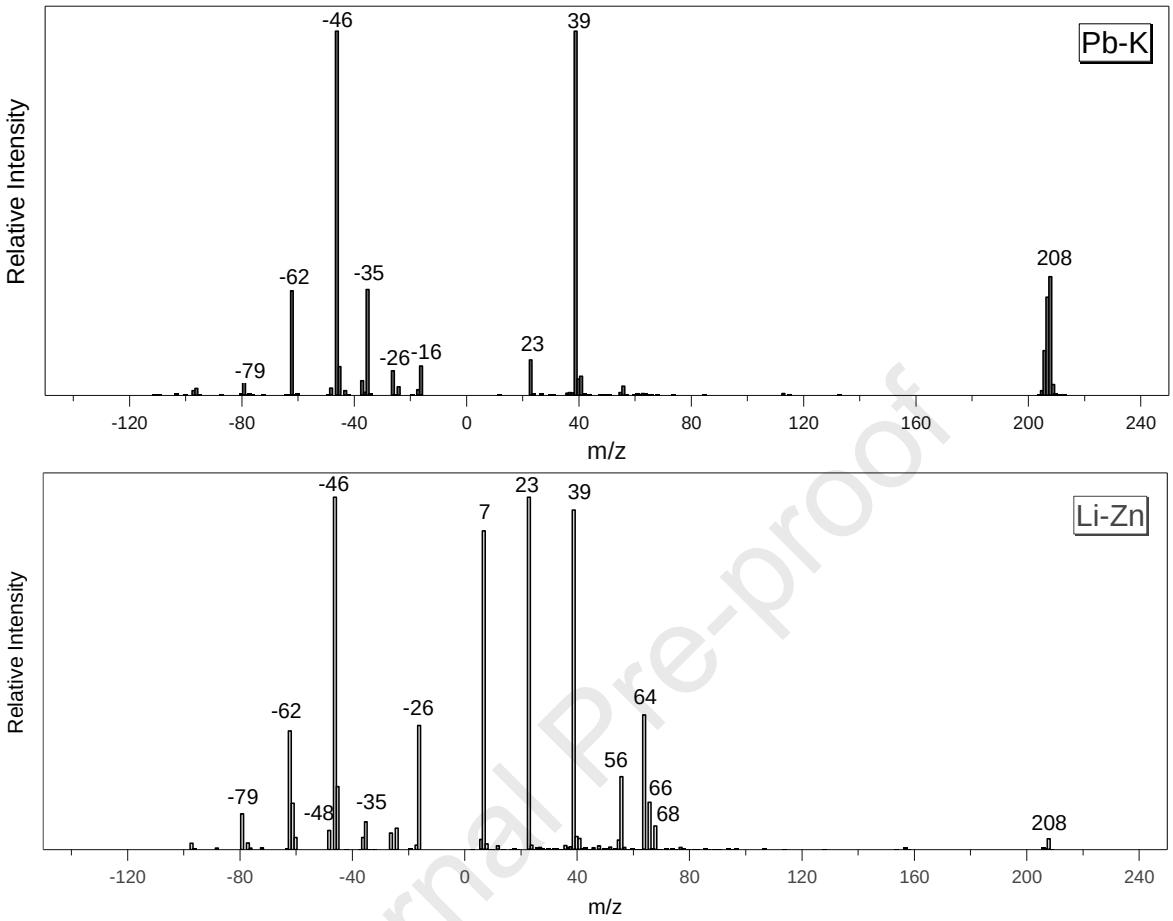

Figure 8: Average mass spectra for Pb-rich and Li-rich metalworking particle classes.

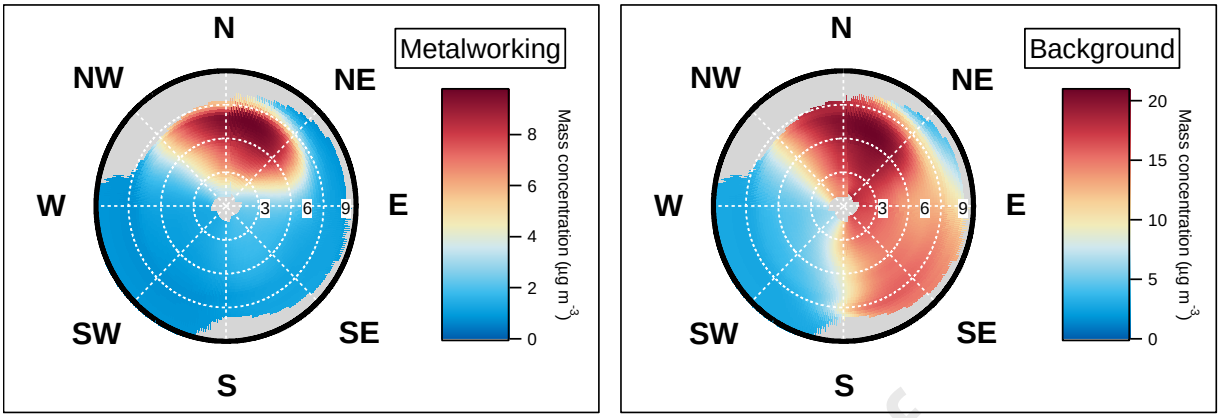

Figure 9: Dependence of concentrations of metalworking and background ATOFMS-derived $PM_{2.5}$ mass concentrations upon local wind speed (m s^{-1}) and wind direction. Periods with wind speed < 1 m s^{-1} are not included in the analysis. Plots generated using the Zefir Toolkit (Petit et al., 2017) running in Igor Pro v6.37 (Wavemetrics Inc.).

Highlights

Particles assigned to a ferromanganese facility and a steelworks based on composition

Metalworking particle composition and mixing state is complex and diverse

Metalworking emissions contributed 17% to $PM_{2.5}$ on average at the receptor site

Metalworking is the dominant source of metals and polycyclic aromatic hydrocarbons

Declaration of interests

☒ The authors declare that they have no known competing financial interests or personal relationships that could have appeared to influence the work reported in this paper.

☐The authors declare the following financial interests/personal relationships which may be considered as potential competing interests: